Path planning of plant protection UAV based on improved A* algorithm under wind conditions

Guanghui Sun, Xianfa Fang*, Licheng Zhu, Yanwei Yuan, Bo Zhao, Zhenhao Han

(*State Key Laboratory of Soil Plant Machine System Technology, Chinese Academy of Agricultural Mechanization Sciences, Beijing 100083, China*)

Abstract: In order to improve safety and reduce energy consumption, a path planning method for the transition of plant protection unmanned aerial vehicles (UAVs) in mountainous and hilly terrain between different plots based on improved A* algorithm was proposed. According to the height of three-dimensional terrain information, a raster voxel map was built. The search space was determined by assigning weights to each grid. The wind cost was introduced into the actual cost function to improve the algorithm. Different weight parameters were set for distance cost and wind cost. Simulation experiments were carried out in the fixed wind field and the variable wind field respectively to obtain the track length and flight time of path planning. The simulation results showed that compared with the classic A* algorithm, the improved A* algorithm could save 9.76%, 7.22% and 11.4% in trajectory, energy and time at the maximum under the condition of fixed wind. Under the condition of variable wind field, the maximum trajectory, energy and time saving percentage was 27.6%, 33.1% and 26.2% respectively compared with the classic A* algorithm. The proposed algorithm could effectively plan a safe and reliable three-dimensional flight path, which provided an effective method for better application of plant protection UAVs in complex hilly terrain.

Keywords: A* algorithm, path-planning, wind vector

DOI: 10.33440/j.ijpaa.20200304.125

Citation: Sun G H, Fang X F, Zhu L C, Yuan Y W, Zhao B, Han Z H. Path planning of plant protection UAV based on improved A* algorithm under wind conditions. Int J Precis Agric Aviat, 2020; 3(4): 31–38.

1 Introduction

In recent years, plant protection unmanned aerial vehicles (UAVs) have developed rapidly and been widely used in mountain orchards[1]. Plant protection UAV usually operated in small areas in mountainous and hilly areas. After the UAV was completed in one orchard, it need to go to the next orchard for plant protection operations[2]. Because of uneven mountain height and complex terrain, fixed height or manual flight could not meet the optimization requirements of safety and energy consumption. In order to improve the working efficiency of agricultural UAV and increase the total working area per unit time, it's necessary to plan a safe and reliable three-dimensional flight path with shorter range and less time from the current working site to the waiting site.

Common path planning methods include artificial potential field method, Dijkstra algorithm, A* algorithm, genetic algorithm, ant colony algorithm, simulated annealing algorithm, particle swarm optimization algorithm, cuckoo algorithm, etc., and these algorithms have also been widely used in unmanned vehicles and robots[3-9]. A* algorithm is one of the most effective classical heuristic search algorithms for the shortest path. Shuai Zhang[10] adopted the method of cyclic node expansion, which made up for the deficiency that the classical A* algorithm could only expand nodes in a specific direction according to a specific step. Yunhong Ma[11] aimed at the complexity of UAV flight environment in low-altitude penetration, comprehensively considering flight height, track length and other weight factors to search for the optimal route. On the basis of considering the gradient of three-dimensional terrain, Dequn Zhao[12] obtained the optimal path in accordance with walking habits by using A* algorithm.

Wind has a great influence on the flight speed of plant protection UAV[13]. In the process of path planning, not only terrain factors should be considered, but also wind field information should be incorporated into the path planning algorithm[14-16]. Nicola Ceccarelli[17] discussed the flight path planning of UAV under the action of constant wind. Based on the cost of flight time, Yaohong Qu[18] used the improved A* search algorithm to search the track under downwind conditions. Aiming at the problem of three-dimensional path planning of UAV in complex mountain environment, an improved A* algorithm for trajectory planning of agricultural UAV under three-dimensional wind field was proposed.

2 Materials and methods

2.1 Environmental modeling

2.1.1 Terrain model

Parameters such as spray volume, spray concentration, operating width, flight speed and flight altitude need not be taken

Received date: 2020-10-30 **Accepted date:** 2020-12-03

Biography: Guanghui Sun, master student, research interests: Path planning of plant protection UAV, Email:sungh27@163.com; **Licheng Zhu**, Senior Engineer, research interests: Mechanical engineering, Email: zhulicheng@caams.org.cn; **Yanwei Yuan**, PhD, Researcher, research interests: Precision agriculture and agricultural machinery measurement and control technology, Email: yyw215@163.com; **Bo Zhao**, PhD , Researcher, research interests: Mechatronics and automatic control, Email: zhaoboshi@126.com; **Zhenhao Han**, doctoral student, research interests: innovative design of mechanical and electrical products, Email: han_zh93@126.com.

*** Corresponding author: Xianfa Fang**, PhD, Professor, research interests: agricultural mechanization, Mailing Address: China Academy of Agricultural Mechanization Sciences, No. 1 Courtyard, Beishatan, Chaoyang District, Beijing 100083, China. Email: fangxf@caams.org.cn

into account in the non-operational process. When flying from the current block to the target block, the constraints are mainly terrain and wind field. Therefore, it is necessary to establish the terrain model[19] and wind field model before route planning.

The classic A* algorithm is a simple global path planning on the two-dimensional plane[20,21]. Some researchers conducted three-dimensional track planning by using function to establish mountain approximate model[22,23]. This modeling method is quite different from the actual situation and is impractical.

According to the measured elevation data of a certain place, a spatial Cartesian coordinate system with longitude as X_e axis, latitude as Y_e axis and height as Z_e axis was established in this paper, which was called the ground coordinate system. The coordinate information of each point was imported into MATLAB to reconstruct 3D. The terrain was the mountain height data in the area of 200 m×200 m. It was stipulated that the height of the lowest point on the map was 0 m, the relative height of the highest point was 196.5 m, and the maximum height of Z_e axis was 200 m. The mathematical model for 3D reconstruction was shown in Figure 1.

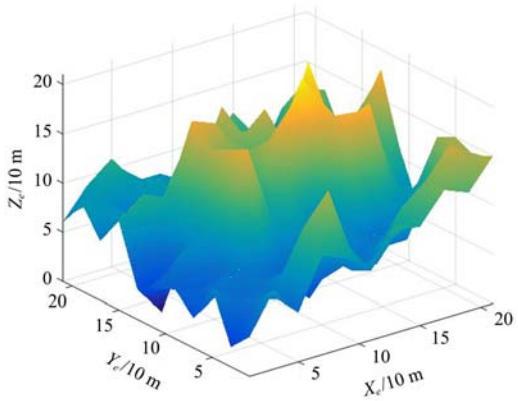

Figure 1 Terrain data

In this paper, the terrain environment was modeled by using grid method. In the three-dimensional space including the starting point and the target point, they were separated into cube elements with the same size along the X_e, Y_e and Z_e axes, and each cube could be determined by the unique coordinate value $Q_i(x_i, y_i, z_i)$. Therefore, path planning problem in three-dimensional space could be transformed into finding the coordinates of a series of points set $\{Q_1, Q_2, Q_3, \ldots, Q_n\}$.

In order to avoid the collision between UAV and hill, this paper presented the height information of hills in the environment grid[24]. The existence state of all meshes could be expressed by a three-dimensional matrix P. Matrix P numerical said the passage of each element in the state, 1 represented no thoroughfare, 0 meant could free passage area.

$Qi(x_i, y_i, z_i)$ represented the location information of the grid, and $P(i, j, k)$ represented the passable state of the grid. When building the model, it was stipulated that:

$$P(i,j,k)=\begin{cases}1, & i=x_i,\ j=y_i,\ k\le z_i+1\\ 1, & i_1=x_i-1,\ i_2=x_i+1,\ j=y_i,\ k\le(0.5*(z_{i1}+z_{i2})+1)\\ 1, & i=x_i,\ j_1=y_i-1,\ j_2=y_i+1,\ k\le(0.5*(z_{j1}+z_{j2})+1)\\ 0, & \text{others}\end{cases} \quad (1)$$

When $i=x_i$, $j=y_i$, the grid at $k\le z_i+1$ was impassable, which could guarantee UAV to keep a safe distance above the ground. In order to avoid the collision between UAV and mountain side, it was stipulated that the flying height of UAV must be higher than the height of adjacent coordinate lines on XOY plane by a certain safety distance. All other points whose P value was not equal to 1 would be used as the search space of A* algorithm, and the goal of path planning was to find a set of optimal coordinates from the starting point to the end point.

2.1.2 Wind vector model

Wind has a great influence on the navigation and control of drones. Different wind directions and wind force have different influences on the speed of UAV. In this paper, an improved A* algorithm was used to plan the flight path of UAV in the wind field to make it fly as downwind as possible to save energy.

Since the trajectory planning in this paper was carried out in three-dimensional space, the online estimation of the wind field needed to obtain the speed of the wind field in all directions in the three-dimensional space. Its vector information could be expressed as:

$$W(x,y,z,t)=\begin{bmatrix}w_{ix}(x,y,z,t)\\ w_{iy}(x,y,z,t)\\ w_{iz}(x,y,z,t)\end{bmatrix} \quad (2)$$

where, $w_{ix}(x,y,z,t)$—the component of the wind speed in the X_e axis in the ground coordinate system, m/s; $w_{iy}(x, y, z, t)$ — the component of the wind speed in the Y_e axis in the ground coordinate system, m/s; $w_{iz}(x,y,z,t)$—the component of the wind speed in the Z_e axis in the ground coordinate system, m/s.

Wind speed could be calculated directly by using GPS speed and vehicle status information [25].Global positioning system provides a direct velocity measurement relative to the earth, accurate to about 0.1 m/s. The wind speed is relative to the ground coordinate system. Each part of the calculation formula is as follows:

$$\begin{bmatrix}w_{ix}\\ w_{iy}\\ w_{iz}\end{bmatrix}=\begin{bmatrix}\dot{x}\\ \dot{y}\\ \dot{z}\end{bmatrix}_{GPS}-T^{-1}\begin{bmatrix}u\\ v\\ w\end{bmatrix} \quad (3)$$

$$T=\begin{bmatrix}\cos\theta\cos\psi & \cos\theta\sin\psi & -\sin\theta\\ \sin\phi\sin\theta\cos\psi-\cos\phi\sin\psi & \sin\phi\sin\theta\sin\psi+\cos\phi\cos\psi & \sin\phi\cos\theta\\ \cos\phi\sin\theta\cos\psi+\sin\phi\sin\psi & \cos\phi\sin\theta\sin\psi-\sin\phi\cos\psi & \cos\phi\cos\theta\end{bmatrix} \quad (4)$$

where, $\dot{x}$ —the velocity component of the drone on the X_e axis of the ground coordinate system, m/s; $\dot{y}$ —the velocity component of the drone on the Y_e axis of the ground coordinate system, m/s; $\dot{z}$ — the velocity component of the drone on the Z_e axis of the ground coordinate system, m/s; T^{-1} — the cosine matrix in the direction of the transformation from body frame $X_bY_bZ_b$ to ground frame $X_eY_eZ_e$[25]; u—the velocity component of the drone on the X_b axis of the body coordinate system, m/s; v — the velocity component of the drone on the Y_b axis of the body coordinate system, m/s; w—the velocity component of the drone on the Z_b axis of the body coordinate system, m/s; θ—the angle between the frame coordinate axis X_b and the ground coordinate axis X_e, rad; ψ—the angle between the frame coordinate axis Y_b and the ground coordinate axis Y_e, rad; ϕ — the angle between the frame coordinate axis Z_b and the ground coordinate axis Z_e, rad.

The matrix T and T^{-1} are inverse matrices. Equations (2), (3) and (4) can estimate the wind speed vector and obtain its components in the ground coordinate system $X_eY_eZ_e$.

2.2 Three-dimensional path planning algorithm

2.2.1 Classic A* algorithm

A* algorithm is a heuristic search algorithm with evaluation

function. When the UAV is moving, the algorithm evaluates the feasibility of the surrounding area, path cost and other parameters. According to the estimated cost, the position of the next target point of UAV is selected until the termination coordination point is found. The mathematical formula is as follows:

$$f(n)=g(n)+h(n) \tag{5}$$

$f(n)$ is the cost estimate of N nodes from the initial coordinate point to the terminating coordinate point, which is called the cost function; $g(n)$is the actually generated value from the initial coordinate point to the node N in the search space; $h(n)$is the estimated algebraic value of the best path from node N to the ending coordinate point, which is called heuristic function.

2.2.2 Improved A* algorithm

In order to reduce energy consumption, when UAV flies at a certain speed, it is necessary to design a flight path with shorter flight path and shorter flight duration. The improved A* algorithm introduces distance energy cost and wind field cost to evaluate the actual power generation $g(n)$. Distance energy cost represents the power consumption caused by the actual flight distance of UAV from the initial node to the extended node. Since the acceleration in the Z_e axis direction during the climb and descent process will cause the UAV to generate additional energy consumption, the distance energy consumption in the horizontal and vertical directions must be calculated separately[26]. The wind field cost indicates the influence of wind speed vector on the direction of extended node. When the included angle between the wind speed vector and the heading direction of UAV is zero, the cost of wind field is the smallest. Therefore, the actually generated value $G(n)$ could be expressed as:

$$G(n)=\lambda_1 D(n)+\lambda_2 W_1(n) \tag{6}$$

$$D(n)=\sum_{i=2}^{n}[r_1(|x_n-x_{n-1}|+|y_n-y_{n-1}|)+r_2|z_n-z_{n-1}|] \tag{7}$$

$$W_1(n)=\sum_{i=2}^{n}|\cos\Omega-1| \tag{8}$$

where, λ_1—the weight of the energy cost for distance; λ_2—the weight of the wind field cost; r_1—energy consumption per unit distance for horizontal motion, J/m; r_2—energy consumption per unit distance for vertical motion, J/m; Ω—the angle between the wind speed vector and the direction of flight speed, rad.

$\lambda_1+\lambda_2=1$. When $\lambda_1=1$, $\lambda_2=0$, the algorithm is classic A* algorithm. According to the parameter setting method in reference[27], r_1=106 J/m, r_2=340 J/m.

In the path planning process, the heuristic function is expressed as the estimated distance energy consumption between the current node and the target point of the drone:

$$H(n)=r_1(|x_l-x_n|+|y_l-y_n|)+r_2|z_l-z_n| \tag{9}$$

where, (x_n, y_n, z_n)—current coordinate; (x_l, y_l, z_l)—target point coordinate

Therefore, the improved A* algorithm can be expressed as:

$$F(n)=\lambda_1 D(n)+\lambda_2 W_1(n)+H(n) \tag{10}$$

In the process of algorithm searching, the position of the next node is determined by finding the minimum value of the current parent node $F(n)$. Record the best expanding direction for each parent node. After finding the end point, traverse backward along the extension direction to get a set of coordinates from the starting point to the end point. Connecting these coordinate points in turn is the planned trajectory.

By determining the search direction and step size, the search efficiency of the algorithm could be improved. In this paper, the size of the environment grid was a 10×10×10 m cube. Therefore, in the process of node expansion, it could be regarded as a particle without considering the yaw angle and the minimum turning radius of UAV in the flight. In three-dimensional space, when searching from the current parent node to the child node, it could be expanded along the three coordinates X_e, Y_e and Z_e of the ground coordinate system. If the step length along each coordinate axis was set to 1, the increment of coordinate values of X_e, Y_e and Z_e axis could be 1, 0 and –1. Since both the starting point and the ending point were known, in order to simplify the searching process and improve the efficiency and real-time performance of the algorithm, a specific direction could be designated as its main searching direction. X_e was the main search direction in this paper. If each child node can only search along the X_e axis, it was impossible to effectively avoid large obstacles. Therefore, during the node expansion, the increment of X_e axis coordinates were specified as 1 and 0, the search direction of Y_e and Z_e coordinates axis were not limited. The schematic diagram of the node to be searched was shown in Figure 2.

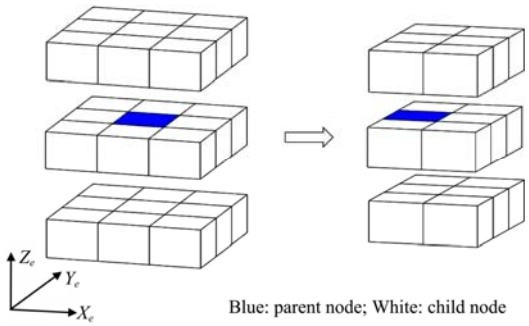

Figure 2 Node to be searched

After the improvement, the number of search nodes of A* algorithm in three-dimensional space is reduced from 26 to 17. Vector d_{ir} represented the search direction and its modulus represented the step size. There were 5 nodes with step length l, 8 nodes with step length $\sqrt{2}l$, and 4 nodes with step length $\sqrt{3}l$.

2.3 Actual flight speed and track length

It is assumed that the UAV flies at a constant speed under the frame coordinate system $X_bY_bZ_b$. Under the action of the wind, due to the different flight directions in the ground coordinate system $X_eY_eZ_e$, there will be different flight speed.

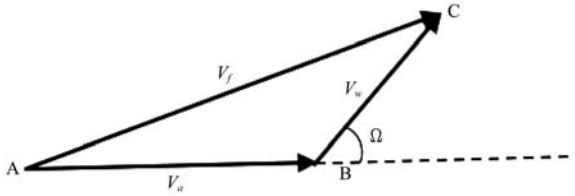

Figure 3 Velocity vector diagram

According to the vector triangle method, $\overrightarrow{AB}$ and $\overrightarrow{BC}$ are the UAV velocity and wind speed vectors. Figure 3 shows the trend of it. The magnitude of the velocity components are F_a and V_w. Vector $\overrightarrow{AC}$ represents the actual ground speed of the UAV, and the magnitude of the velocity V_f is:

$$V_f=\sqrt{V_a^2+V_w^2-2V_aV_w\cos\Omega} \tag{11}$$

where, V_f—ground speed of the UAV, m/s; V_a—airspeed of the UAV, m/s; V_w—wind speed, m/s.

Assuming that the airspeed of UAV remains constant, its actual flying speed will be affected by the wind. When UAV flies from the current node to the next node, the actual flight distance is:

$$H(n)=\sqrt{(x_{n+1}-x_n)^2+(y_{n+1}-y_n)^2+(z_{n+1}-z_n)^2} \tag{12}$$

The actual flight time is:

$$T_n = \frac{H(n)}{V_f} \tag{13}$$

The total length of the track is:

$$F(D) = \sum_{i=1}^{n-1} H(n) \tag{14}$$

The actual total flight time is:

$$F(T) = \sum_{i=1}^{n-1} T_n \tag{15}$$

Since the energy consumption H of plant protection UAV is proportional to the flight time $F(T)$. The cost function could be expressed as follows[28]:

$$\min H = kF(T) \tag{16}$$

where, k— the proportional coefficient.

So shorter flight time means better trajectory.

2.4 Simulation Test

When the starting and ending positions are known, the quality of the track is mainly expressed by such parameters as the length of the flight, power consumption, flight time and the degree of threat. In this paper, limiting factors such as terrain were excluded from the search range of the algorithm, and the planned path was considered safe and feasible. In order to compare the advantages and disadvantages of this algorithm with the classic algorithm, the track length, distance energy consumption and flight time were analyzed.

2.4.1 Fixed wind field

It was assumed that the airspeed of UAV was V_a=6 m/s, which remained unchanged. The starting point was Q_s=[1, 6, 7], the ending point was Q_g=[21, 18, 18], and the direction vector connecting the starting point to the ending point was v= [20, 12, 11]. When the angle between the wind speed vector and vector v was less than 90 degrees, it was downwind; when the included angle between the wind speed vector and vector v was greater than 90 degrees, it was upwind. There were downwind and upwind fixed wind fields that have been set respectively in this experiment. The magnitude of downwind field vector was set as V_w=[1 1 1], and the magnitude of upwind field vector was set as V_w=[–1 –1 –1]. Under different λ_1 and λ_2 parameter values, the flight path length and flight time between the improved A* algorithm and the classic A* algorithm under different weights were compared.

2.4.2 Variable wind field

In actual flight, the wind field is not constant. Therefore, path planning should be carried out according to the real-time changing wind field. The UAV airspeed was assumed to be V_a=6 m/s and kept constant. The starting point was Q_s'=[5 5 8], the ending point was Q_g'=[20 20 15], and the direction vector connecting the starting point to the ending point was v'=[15 15 7].

Wind speed vectors at different times can be represented by a set of three-dimensional vectors $W(x, y, z)$.

$$W(x,y,z) = \begin{bmatrix} 1 & 1 & 1 \\ -1 & -1 & -1 \\ 1 & -1 & 0 \\ 1 & 1 & 0 \end{bmatrix}$$

Each row represented the wind speed vector at a given time, and each element represented its component expressed in m/s along the X_e, Y_e and Z_e axes. The first line represented the wind speed vector under downwind conditions, and the second line represented the wind speed vector under upwind conditions. Because the product with vector v' was zero, the third and fourth lines could represent wind speed vector under lateral wind conditions. Assuming that the wind vector changed at the moment of t = 20 s. Different wind fields were set up from upwind to lateral wind, downwind to lateral wind, lateral wind to upwind, and lateral wind to downwind, respectively. Then, the classical A * algorithm was compared with the improved A* algorithm under different weights.

3 Results and discussion

3.1 Analysis of fixed wind field results

Simulation 1- 3 in Table 1 was the trajectories planned by the classical A* algorithm under the conditions of no wind, downwind and upwind. Its length was 354.35 m, and its distance energy consumption was 5758.2j. Because of the actual flying speed of UAV is higher than airspeed when downwind, it could be seen from the flight time that the flight time become shorter under downwind conditions and increased under upwind conditions. Therefore, the wind vector had a great influence on the actual flight time of UAV, so the influence of wind should be considered in the process of path planning.

Table 1 Planned path and flight time of the classic A* algorithm

No.	Wind vector /m·s^{-1}	Track length /m	Distance energy consumption/J	Flight time /s
1	[0 0 0]	354.35	5758.2	59.058
2	[1 1 1]	354.35	5758.2	48.692
3	[–1 –1 –1]	354.35	5758.2	72.617

Table 2 Planned path and flight time under downwind conditions

No.	Parameter	Wind vector /m·s^{-1}	Track length /mm	Distance energy consumption/J	Flight time /s	Percentage saving of track/%	Percentage saving of energy/%	Percentage saving of time/%
1	λ_1=0.8, λ_2=0.2	[1 1 1]	328.49	5412.4	44.457	7.30	6.01	8.70
		[–1 –1 –1]	328.49	5412.4	68.456	7.30	6.01	5.73
2	λ_1=0.6, λ_2=0.4	[1 1 1]	320.71	5342.2	43.267	9.49	7.22	11.1
		[–1 –1 –1]	327.53	5444.2	68.413	7.57	5.45	5.79
3	λ_1=0.4, λ_2=0.6	[1 1 1]	320.70	5342.2	43.267	9.49	7.22	11.1
		[–1 –1 –1]	320.70	5342.2	67.534	9.49	7.22	7.00
4	λ_1=0.2, λ_2=0.8	[1 1 1]	319.74	5374.0	43.126	9.76	6.67	11.4
		[–1 –1 –1]	336.31	5543.6	70.348	5.09	3.73	3.12
5	λ_1=0, λ_2 =1	[1 1 1]	328.02	5458.8	44.481	7.43	5.20	8.65
		[–1 –1 –1]	358.27	6876.2	74.252	–1.11	–19.4	–2.25

Table 2 showed the planning trajectories of the improved A* algorithm under different parameters. Compared with the data in Table 1, it could be seen that the flight path length, distance energy consumption and flight time were all reduced under downwind conditions compared with the planning without considering wind field information. When λ_1=0.2, λ_2=0.8, the shortest track length was 319.74 m ,and the total flight time was 42.9861 s. Compared with the classic A* algorithm, the track and time were saved by 9.76% and 11.4% ,respectively. However, the distance energy consumption was not the lowest under this parameter. When λ_1=0.4, λ_2=0.6, the distance generated the lowest energy consumption was 5342.2j. At this point, the saving of energy was 7.22%.

Under upwind conditions: When λ_1=0, λ_2=1, the distance energy consumption coefficient was zero, so the planned path was seriously unreasonable. Under this parameter, the track length, distance energy consumption and flight time all increase. When λ_1=0.4, λ_2=0.6, the shortest track length was 320.70 m and the distance energy consumption was 5342.2j. At this time, the total flight time was 67.534 s. Compared with the classic A* algorithm, the saving of trajectory, energy consumption and time percentage were 9.49%, 7.22% and 7.00%, respectively.

The results showed that the improved A* algorithm was better than the classic A* algorithm in planning path under the condition of fixed wind field. The optimal trajectory planned under the conditions of no wind, downwind and upwind were shown in the red, purple and yellow lines in Figure 4.

3.2 Analysis of variable wind field results

(1) Upwind - lateral wind conditions

Under the upwind - lateral wind conditions, the track length planned by the classic A* algorithm was 371.41 m, and the energy consumption was 6667.8j. At the moment of t=20 s, in the wind field where the wind vector changed from the upwind [–1 –1 –1] to the lateral wind [–1 1 0], the flight time was 67.182 s. In the wind field where the wind velocity vector changed from the lateral wind [1 –1 0] to the headwind [–1 –1 –1], the flight time was 65.358 s. The planning path data in Table 3 was contrasted with this data.

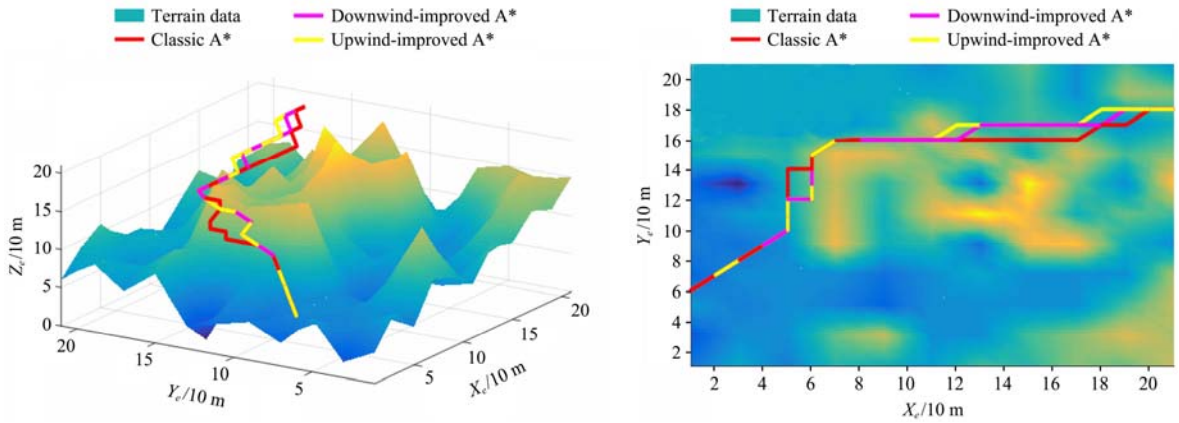

Figure 4 Track planning for fixed wind field

Table 3 Planned path and flight time under upwind - lateral wind conditions

No.	Parameter	Wind vector /m·s^{-1}	Track length /mm	Distance energy consumption/J	Flight time /s	Percentage saving of track/%	Percentage saving of energy/%	Percentage saving of time/%
1	λ_1=0.8, λ_2=0.2	[–1 –1 –1] → [–1 1 0]	369.49	6731.4	66.905	0.517	–0.954	0.412
		[1 –1 0] → [–1 –1 –1]	370.45	6699.6	65.063	0.258	–0.477	0.451
2	λ_1=0.6, λ_2=0.4	[–1 –1 –1] → [–1 1 0]	354.38	6685.0	64.323	4.59	–0.258	4.26
		[1 –1 0] → [–1 –1 –1]	369.49	6731.4	64.769	0.517	–0.954	0.901
3	λ_1=0.4, λ_2=0.6	[–1 –1 –1] → [–1 1 0]	341.70	6519.4	62.859	8.00	2.23	6.43
		[1 –1 0] → [–1 –1 –1]	335.84	6455.8	58.047	9.58	3.18	11.2
4	λ_1=0.2, λ_2=0.8	[–1 –1 –1] → [–1 1 0]	279.74	4692.6	52.672	24.7	29.6	21.6
		[1 –1 0] → [–1 –1 –1]	334.88	6487.6	57.752	9.84	2.70	11.6
5	λ_1=0, λ_2 =1	[–1 –1 –1] → [–1 1 0]	315.84	6501.2	58.946	15.0	2.50	12.3
		[1 –1 0] → [–1 –1 –1]	309.02	6141.8	53.152	16.8	7.89	18.7

From upwind to lateral wind, When λ_1=0.2, λ_2=0.8, the shortest track length was 279.74 m and the energy consumption of this distance was 4692.6j. At this time, the total flight time was 52.672 s. Compared with the classic A* algorithm, the saving of track, energy consumption and time percentage were 24.7%, 29.6% and 21.6%, respectively. When {λ_1=0.8, λ_2=0.2}, {λ_1=0.6, λ_2=0.4}, the track length and flight time decreased slightly, but the energy consumption increased. Because there are many climbing and descending processes in the planning, it would increase power consumption.

From lateral wind to upwind, When λ_1=0, λ_2=1, the shortest track length was 309.02 m and the energy consumption of this distance was 6141.8j. At this time, the total flight time was 53.152 s. Compared with the classic A* algorithm, the saving of track, energy consumption and time percentage were 16.8%, 7.89% and 18.7%, respectively.

Under the upwind-lateral wind conditions, the three-dimensional planned trajectory and its projection on the XY plane were shown in Figure 5. Among them, red represented the planned trajectory without considering the wind field information, and yellow indicated the planned track with optimal parameters after considering the wind field information.

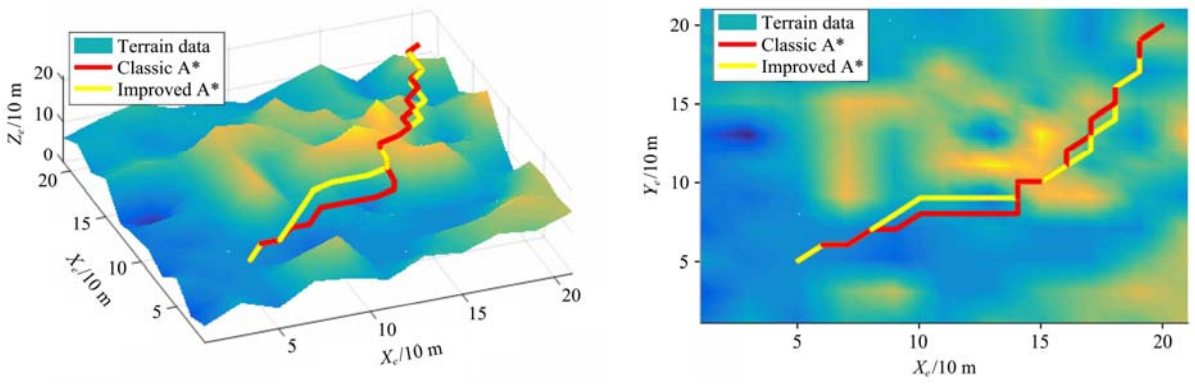

a. Lateral wind [1 –1 0] to the upwind [–1 –1 –1]

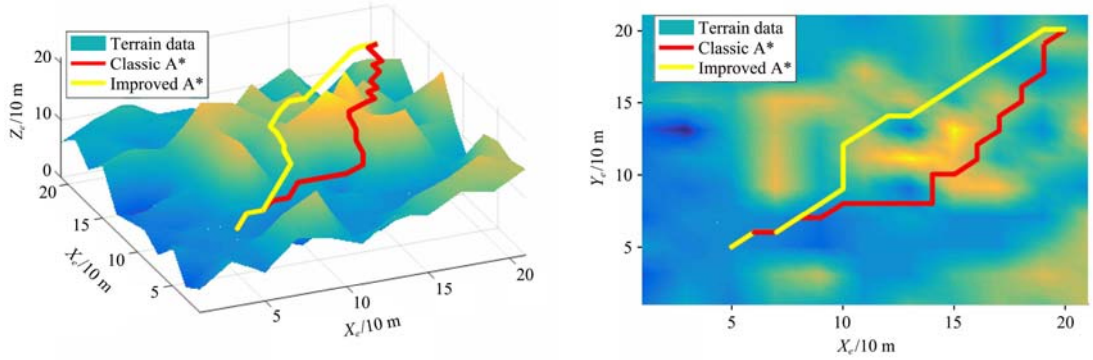

b. Upwind [–1 –1 –1] to the lateral wind [–1 1 0]

Figure 5 Track planning with upwind - lateral wind conditions

Table 4 Planned path and flight time under downwind - lateral wind conditions

No.	Parameter	Wind vector /m·s^{-1}	Track length /mm	Distance energy consumption/J	Flight time /s	Percentage saving of track/%	Percentage saving of energy/%	Percentage saving of time/%
1	λ_1=0.8, λ_2=0.2	[1 1 1] → [–1 1 0]	369.49	6731.4	54.627	0.517	–0.954	0.505
		[1 –1 0] → [1 1 1]	356.31	6621.4	54.257	4.07	0.695	4.77
2	λ_1=0.6, λ_2=0.4	[1 1 1] → [–1 1 0]	355.34	6653.2	51.661	4.33	0.219	5.91
		[1 –1 0] → [1 1 1]	356.31	6621.4	54.257	4.07	0.695	4.77
3	λ_1=0.4, λ_2=0.6	[1 1 1] → [–1 1 0]	274.85	4597.2	41.410	26.0	31.1	24.6
		[1 –1 0] → [1 1 1]	328.52	6339.2	49.319	11.5	4.93	13.4
4	λ_1=0.2, λ_2=0.8	[1 1 1] → [–1 1 0]	268.99	4463.4	40.500	27.6	33.1	26.2
		[1 –1 0] → [1 1 1]	335.84	6455.8	50.475	9.58	3.18	11.4
5	λ_1=0, λ_2 =1	[1 1 1] → [–1 1 0]	315.84	6501.2	45.535	15.0	2.50	17.1
		[1 –1 0] → [1 1 1]	309.02	6141.8	45.676	16.8	7.89	19.8

(2) Downwind - lateral wind conditions

Under the downwind - lateral wind conditions, the track length planned without considering the wind field information was 371.41 m, and the energy consumption was 6667.8 J. At the moment of t=20 s, in the wind field where the wind vector changed from downwind [1 1 1] to lateral wind [–1 1 0], the flight time was 54.904 s. In the wind field where the wind vector changed from lateral wind [1 –1 0] to downwind [1 1 1], the flight time was 56.974 s. The planning path data in Table 4 was contrasted with this data.

From downwind to lateral wind, When λ_1=0.2, λ_2=0.8, the shortest track length was 268.99 m and the energy consumption of this distance was 4463.4j. At this time, the total flight time was 40.500 s. Compared with the classic A* algorithm, the saving of track, energy consumption and time percentage were 27.6%, 33.1% and 26.2%, respectively.

From lateral wind to downwind, When λ_1=0, λ_2=1, the shortest track length was 309.02 m and the energy consumption of this distance was 6141.8j. At this time, the total flight time was 45.676 s. Compared with the classical A* algorithm, the saving of track, energy consumption and time percentage were 16.8%, 7.89% and 19.8% respectively. When {λ_1=0.8, λ_2=0.2}, {λ_1=0.6, λ_2=0.4}, the planned trajectory were the same despite the different parameters. This is because the algorithm in this paper expanded the nodes according to the size relation of the cost estimation. Here, although the weight of the wind field cost and the distance cost were different, the size relationship of the surrounding nodes was identical. Therefore, the same track could be obtained under different weights.

Under the downwind - lateral wind conditions, the three-dimensional planning track and its projection on the XY plane were shown in Figure 6. Among them, red represented the planned trajectory without considering the wind field information, and yellow indicated the planned track with optimal parameters after considering the wind field information.

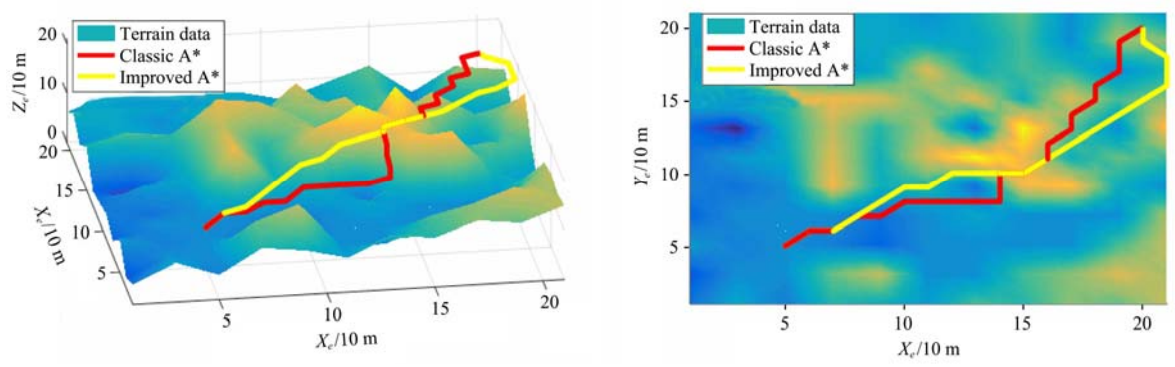

a. Lateral wind [1 –1 0] to downwind [1 1 1]

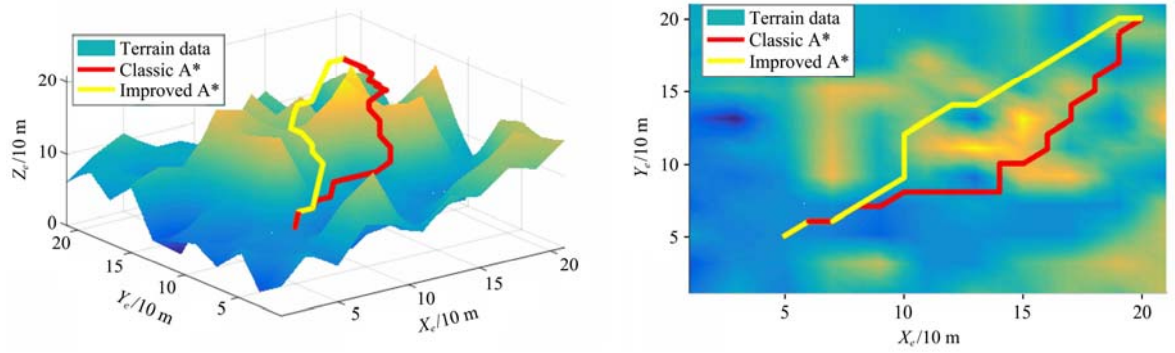

b. Downwind [1 1 1] to lateral wind [–1 1 0]

Figure 6 Downwind - lateral wind planning track

4 Conclusions

(1) An improved A* algorithm was proposed to solve the problem of continuous operation among multiple plots in mountainous areas of agricultural drone which combine wind field vector information and search direction. The improved A* algorithm proposed in this paper could obtain a better flight path of plant protection UAV and reduce planning time, path length and total flight time.

(2) By determining the main search direction in the three-dimensional space, the search node was reduced from the original 26 nodes to 17 nodes, which could effectively reduce the number of searches and improve the efficiency of the algorithm.

(3) Integrating the wind cost into the actual cost function to improve the cost function could make the nodes of the path more inclined to search downwind. It could effectively reduce the length of the planning path and the flight time. Experiments were conducted
in fixed and variable wind fields. The results showed that compared with the classic A* algorithm, the total flight path length, energy consumption and the total flight time could be saved by 27.6%, 33.1% and 26.2%, respectively.

Acknowledgments

We deeply thank for the National Key Research and Development Program of China (No. 2016YFD0200702).

[References]

[1] Lan Y B, Chen S D. Current status and trends of plant protection UAV and its spraying technology in China. Int J Precis Agric Aviat, 2018; 1(1): 1–9. doi: 10.33440/j.ijpaa.20180101.0002

[2] Hu J, Yang J C. Application of distributed auction to multi-UAV task assignment in agriculture. Int J Precis Agric Aviat, 2018; 1(1): 44–50. doi: 10.33440/j.ijpaa.20180101.0008

[3] Gu Q, Dou F Q, Ma F. Energy Optimal Path Planning of Electric Vehicle Based on Improved A* Algorithm. Transactions of the Chinese Society for Agricultural Machinery, 2015, 46(12): 316–322. doi: 10.6041/j.issn.1000-1298.2015.12.043 (in Chinese)

[4] Li Q, Xie S J, Tong X H, et al. A self-adaptive genetic algorithm for the shortest path planning of vehicles and its comparison with Dijkstra and A*algorithms. Journal of University of Science and Technology Beijing, 2006, 28(11): 1082–1086. doi: 10.3321/j.issn:1001-053X.2006.11.017 (in Chinese)

[5] Zhang J Y, Zhao Z P, Liu D.A path planning method for mobile robot based on artificial potential field. Journal of Harbin Institute of Technology, 2006, 38(8): 1306–1309. doi: 10.3321/j.issn:0367-6234.2006.08.026 (in Chinese)

[6] Shi E X, Chen M M, Li J, et al. Research on method of global path-planning for mobile robot based on ant-colony algorithm. Transactions of the Chinese Society for Agricultural Machinery, 2014, 45(6): 53–57. doi: 10.6041/j.issn.1000-1298.2014.06.009 (in Chinese)

[7] He L Y, Yang T W, Wu C Y, et al. Optimization of Replugging Tour Planning Based on Greedy Genetic Algorithm. Transactions of the Chinese Society for Agricultural Machinery, 2017, 48(05): 36–43. doi: 10.6041/j.issn.1000-1298.2017.05.004 (in Chinese)

[8] Yuan J Q, Li S, Wu Y F, et al. Robot Path Planning Method Based on Simulated Annealing Ant Colony Algorithm. Computer Integrated Manufacturing Systems, 2019, 36(10): 329–333. doi: 10.3969/j.issn.1006-9348.2019.10.068 (in Chinese)

[9] Yuan Y W, Zhang X C, Hu X A. Algorithm for optimization of apple harvesting path and simulation[J]. Transactions of the SAE, 2009, 25(04): 141–144. (in Chinese)

[10] Zhang S, Li X R, Zhang P, et al. UAV path planning based on improved A* algorithm. Flight Dynamics, 2016, 34(03): 39–43. doi: 10.13645/j.cnki.f.d.20160110.007 (in Chinese)

[11] Ma Y H, Zhang H, Qi L R, et al. A 3D UAV Path Planning Method Based on Improved A* Algorithm. Electronics Optics & Control, 2019, 26(10): 22–25. doi: 10.3969/j.issn.1671-637X.2019.10.005 (in Chinese)

[12] Zhao D Q, Duan J Y, Chen P Y, et al. Optimal Path Planning for 3D Map Based on A ✲ Algorithm. Computer Systems & Applications, 2017, 26(07): 146–152. doi: 10.15888/j.cnki.csa.005859 (in Chinese)

[13] Li J Y, Wu H, Hu X D, Fan G A, Li Y F, Long B, Wei X, Lan Y B. Method for establishing the UAV-rice vortex 3D model and extracting spatial parameters. Int J Precis Agric Aviat, 2020; 3(2): 56–64. doi: 10.33440/j.ijpaa.20200302.84

[14] Shiga K, Kumon M. Online path optimization for unmanned aerial vehicles under steady wind. IEEE/SICE International Symposium on System Integration. IEEE, 2012. doi: 10.1109/sii.2012.6427369

[15] Rucco A, Aguiar A P, Pereira F L, et al. 2015. A Predictive Path-Following Approach for Fixed-Wing Unmanned Aerial Vehicles in Presence of Wind Disturbances. Robot 2015: Second Iberian Robotics Conference, 623–634. doi: 10.1007/978-3-319-27146-0_48

[16] Ailliot P, Monbet V, Prevosto M. An autoregressive model with time-varying coefficients for wind fields. Environmetrics, 2006, 17(2): p.107–117. doi: 10.1002/env.753

[17] Ceccarelli N, Enright J J, Frazzoli E, et al. Micro UAV Path Planning for Reconnaissance in Wind. 2007 American Control Conference. doi: 10.1109/acc.2007.4282479

[18] Qu Y H, Xiao Z B, Yuan D L. An Effective Method of UAV Flight Path Planning On-Line in Wind Field Using Improved A* Searching Algorithm. Journal of Northwestern Polytechnical University, 2012, 30(04): 576–581. doi: 10.3969/j.issn.1000-2758.2012.04.018 (in Chinese)

[19] Wu J W, Xue X Y, Zhang S C, Qin W C, Chen C, Sun T. Plant 3D reconstruction based on LiDAR and multi-view sequence images. Int J Precis Agric Aviat, 2018; 1(1): 37–43. doi: 10.33440/j.ijpaa.20180101.0007

[20] Pan S Y, Xu X R. 2D and 3D Robot Path Planning Based on the A* Algorithm. Journal of Jing gangshan University (Natural Sciences Edition), 2015, 36(05): 84–88. doi: 10.3969/j.issn.1674-8085.2015.05.016 (in Chinese)

[21] Lu L, Wang J Q, Zong C X, et al. Simulation of 3D path planning approach for quad-rotor helicopter based on A* algorithm. Journal of Hefei University of Technology(Natural Science), 2017, 40(03): 304–309. doi: 10.3969/j.issn.1003-5060.2017.03.004 (in Chinese)

[22] Zhao F, Yang W, Yang C X, et al. UAV three-dimensional dynamic route planning and guidance control research. Computer Engineering and Applications, 2014, 50(2): 58–64. doi: 10.3778/j.issn.1002-8331.1308-0305 (in Chinese)

[23] Zhang D S, Huang C Q, Ding D L, et al. Attacking Track Calculation of UAVs Based on A* Algorithm[J]. Electronics Optics & Control, 2011, 18(03): 18–20+65. doi: 10.3969/j.issn.1671-637X.2011.03.005 (in Chinese)

[24] Wang LL, Xiao WW, Qi Y, Gao Q C,Li L, YanKT, Zhang Y L, Lan Y B. Farmland human-shape obstacles identification based on Viola-Jones Algorithm. Int J Precis Agric Aviat, 2020; 3(3): 35–40. doi: 10.33440/j.ijpaa.20200303.99

[25] Pei S Y, Wang S Z, Zhang H H, Zhu H. Methods for monitoring and controlling multi-rotor micro-UAVs position and orientation based on LabVIEW. Int J Precis Agric Aviat, 2018; 1(1): 51–58. doi: 10.33440/j.ijpaa.20180101.0009

[26] Goss K, Musmeci R, Silvestri S. Realistic Models for Characterizing the Performance of Unmanned Aerial Vehicles. 2017 26th International Conference on Computer Communication and Networks (ICCCN). doi: 10.1109/icccn.2017.8038444

[27] Zhang Q Q, Xu W W, Zhang H H, et al. Path planning for logistics UAV in complex low-altitude airspace. Journal of Beijing University of Aeronautics and Astronautics: 1-15[2020-06-09]. doi: 10.13700/j.bh.1001-5965.2019.0455 (in Chinese)

[28] Christian B. Ant colony optimization: Introduction and recent trends. Physics of Life Reviews, 2005, 2(4): 353–373. doi: 10.1016/j.plrev.2005.10.001